




# Functional Profiling of Chondrogenically Induced Multipotent Stromal Cell Aggregates Reveals Transcriptomic and Emergent Morphological Phenotypes Predictive of Differentiation Capacity

JOHNNY LAM , IAN H. BELLAYR, ROSS A. MARKLEIN, STEVEN R. BAUER, RAJ K. PURI, KYUNG E. SUNG

**Key Words.** Adult stem cells • Chondrogenesis • Gene expression • Mesenchymal stem cells • Microarray • Stromal cells • Tissue engineering • Transforming growth factor  $\beta$

<sup>a</sup>Division of Cellular and Gene Therapies, Center for Biologics Evaluation and Research, Food and Drug Administration, Silver Spring, Maryland, USA

Correspondence: Kyung E. Sung, Division of Cellular and Gene Therapies, Center for Biologics Evaluation and Research, Food and Drug Administration, Silver Spring, MD 20993, USA; e-mail: kyung.sung@fda.hhs.gov

Received March 20, 2018; revised May 7, 2018; accepted for publication May 17, 2018; first published August 7, 2018.

<http://dx.doi.org/10.1002/sctm.18-0065>

This is an open access article under the terms of the Creative Commons Attribution-NonCommercial-NoDerivs License, which permits use and distribution in any medium, provided the original work is properly cited, the use is non-commercial and no modifications or adaptations are made.

## ABSTRACT

Multipotent stromal cells (MSCs) are an attractive cell source for bone and cartilage tissue repair strategies. However, the functional heterogeneity of MSCs derived from different donors and manufacturing conditions has limited clinical translation, emphasizing the need for improved methods to assess MSC chondrogenic capacity. We used functionally relevant morphological profiling to dynamically monitor emergent morphological phenotypes of chondrogenically induced MSC aggregates to identify morphological features indicative of MSC chondrogenesis. Toward this goal, we characterized the morphology of chondrogenically stimulated MSC aggregates from eight different human cell-lines at multiple passages and demonstrated that MSC aggregates exhibited unique morphological dynamics that were both cell line- and passage-dependent. This variation in 3D morphology was shown to be informative of long-term MSC chondrogenesis based on multiple quantitative functional assays. We found that the specific morphological features of spheroid area, radius, minimum feret diameter, and minor axis length to be strongly correlated with MSC chondrogenic synthetic activity but not gene expression as early as day 4 in 3D culture. Our high-throughput, nondestructive approach could potentially serve as a tool to identify MSC lines with desired chondrogenic capacity toward improving manufacturing strategies for MSC-based cellular products for cartilage tissue repair. *STEM CELLS TRANSLATIONAL MEDICINE* 2018;7:664–675

## SIGNIFICANCE STATEMENT

Despite their regenerative potential, the functional heterogeneity of multipotent stromal cells (MSCs) derived from different donors and manufacturing conditions has limited clinical translation, emphasizing the need for improved methods to assess MSC differentiation ability. Utilizing functionally relevant morphological profiling to dynamically monitor emergent morphological phenotypes of chondrogenically induced MSC aggregates, this work demonstrated that MSC aggregates derived from different donors showed unique morphological dynamics that were informative of long-term chondrogenic differentiation capacity. Furthermore, transcriptomic analysis revealed that the gene expression of undifferentiated MSCs also correlated with chondrogenic potential. Overall, a well-defined tool is presented for the early estimation of MSC chondrogenesis.

## INTRODUCTION

Articular cartilage is a dynamic, stress-bearing connective tissue that functions to facilitate the frictionless articulation of adjoining bones within synovial joints. The avascular, but highly hydrated, cartilage matrix comprises a hierarchical structure of proteoglycans and collagens organized to provide its characteristic viscoelastic

and compressive mechanical properties [1, 2]. The cellular constituents of cartilage are chondrocytes, which are specialized extracellular matrix-producing cells with low proliferative capacity [3]. However, damaged articular cartilage (due to trauma or disease) remains one of the most difficult tissues to repair due to its low endogenous capacity for regeneration and continues to be a leading cause of disability

worldwide [4]. Furthermore, the successful outcome of cell-based therapies for cartilage repair requiring the use of chondrocytes, such as autologous chondrocyte implantation (ACI), is often marred by the propensity of chondrocytes to dedifferentiate during ex vivo expansion [5] as well as the significant donor morbidity associated with their harvest.

To mitigate such problems associated with ACI, multipotent stromal cells (MSCs) have become an attractive alternative cell source due to their capacity for self-renewal, ease of isolation, and chondrogenic differentiation potential [6, 7]. Unlike adipogenesis and osteogenesis, the chondrogenic induction of MSCs typically requires the use of a 3D culture format allowing for cell aggregation [8]. Many research groups have successfully induced chondrogenic differentiation of MSCs in vitro via high-density 3D culture platforms, which allow the formation of 3D microtissues by promoting intimate cell–cell contacts [9–11]. This 3D microtissue model is thought to recapitulate aspects of developmental processes during mesenchymal condensation that precede cartilage formation [12, 13]. Although widely recognized, this biologically inspired design has only recently been incorporated into tissue engineering strategies for enhancing cartilage repair in vivo [14–16]. While abundant research demonstrates their therapeutic potential in the context of cartilage repair, a major challenge to successful clinical translation that remains is MSC functional heterogeneity [17]. Significant cell-to-cell heterogeneity exists within MSC populations derived from different donors and manufacturing processes, which results in substantial differences in functional capacity and has thus limited their overall therapeutic effectiveness and clinical potential [18].

In order to better understand and address MSC functional heterogeneity, functionally relevant morphological profiling (FRMP) has been previously used to identify morphological features predictive of MSC functional capacity [19]. Indeed, effective analytical tools such as FRMP have successfully linked phenotypic readouts such as cell morphology to MSC osteogenic potential [20, 21]. Under osteogenic stimulation in 2D, MSCs displayed more uniform actin fiber rearrangement, greater cell spreading area, decreased aspect ratios, as well as increased focal adhesions [22]. These morphological and cytoskeletal “profiles” of MSCs could then be used to predict the capacity of an MSC line to undergo osteogenic differentiation. An application of this methodology demonstrated that certain morphological features of MSCs exposed to osteogenic stimuli were highly predictive of their ability for eventual mineral deposition [20]. It was further revealed in another investigation that distinct morphological changes of MSCs exposed to the inflammatory cytokine interferon- $\gamma$  were highly correlated to MSC ability to suppress T cell activation, highlighting the utility of using functionally relevant stimuli for developing predictive bioassays [23]. While the morphological profiling of single cells in 2D can reveal heterogeneous responses to external stimuli, there still remains significant need for quantitative methods to assess MSC functional heterogeneity within physiologically relevant 3D model systems. The adaptation of a functionally relevant approach for the estimation of MSC chondrogenic capacity via the interrogation of their 3D aggregate morphology would provide a useful tool for bridging the gap between understanding MSC heterogeneity and clinical translation for cartilage repair.

Here, we use a nondestructive approach to quantify high-dimensional morphological features of chondrogenically stimulated

MSC aggregates and show differences in morphological dynamics related to cell lines from different donors and cell line passage. We hypothesize that such differences in MSC aggregate morphology, which represents a functionally relevant 3D phenotypic readout, are early indicators of chondrogenic differentiation capacity of MSC lines. By establishing linear relationships between metrics of MSC aggregate morphology and multiple quantitative chondrogenic outcomes, we show that emergent 3D aggregate phenotypes correlate strongly with long-term chondrogenesis assessed through cell content, gene expression, and protein expression. We also identified a number of genes from the transcriptomic analysis of undifferentiated MSCs that correlated with their chondrogenic differentiation capacity. These findings lay a foundation for better understanding MSC functional heterogeneity in the context of chondrogenesis and represent a generalizable analytical approach for quickly assessing cell quality and guiding cell manufacturing strategies that could be applied to additional cell types and therapeutic applications.

## MATERIALS AND METHODS

### MSC Culture and Expansion

Human bone marrow-derived MSCs were obtained from eight different donors purchased from RoosterBio (RB9, RB12, RB14, RB16; Frederick, MD) at passage 1 (P1), Lonza (8F560, 167696; Walkersville, MD) at passage 2 (P2), and AllCells (PCBM1632, PCBM1641; Alameda, CA) at P2 (see Fig. 1 for donor specifications). MSCs were cultured and expanded following previously established procedures [20]. P2 RoosterBio MSCs and P3 Lonza/AllCells MSCs were used to represent early passage (EP) groups as the MSCs were derived after one passage from the indicated passage at purchase. P5 MSCs for all groups were used to represent late passage (LP).

### MSC Spheroid Culture and Chondrogenic Differentiation

To generate MSC aggregates for spheroid culture, MSCs derived from each donor were trypsinized and then resuspended in chondrogenic induction medium (high glucose Dulbecco's MEM supplemented with 10 ng/ml TGF- $\beta$ 3 (Peprotech, Rocky Hill, NJ), ITS + Premix (6.25  $\mu$ g/ml insulin, 6.25  $\mu$ g/ml transferrin, 6.25  $\mu$ g/ml selenious acid, 5.35  $\mu$ g/ml linoleic acid, and 1.25  $\mu$ g/ml bovine serum albumin) (Corning, Corning, NY), 50 mg/l ascorbic acid-2-phosphate,  $10^{-7}$  M dexamethasone, 1% L-glutamine, and 1% penicillin–streptomycin) at a concentration of  $10^5$  cells/150  $\mu$ l. 150  $\mu$ l of cell suspension was added to each well of ultralow-attachment 96-well plates (Costar; Corning) and then centrifuged at 250g for 5 minutes. MSC aggregates were incubated in parallel in a humidified chamber at 37°C and 5% CO<sub>2</sub> and cultured for 3 weeks. The chondrogenic induction medium was changed at 24 hours and then at every other day following aggregate formation. At day 21, samples were retrieved for analyses. A minimum of 10 individual spheroids were generated for each experimental group.

### Quantitative Morphological Analysis of MSC Aggregates

MSC aggregates (Fig. 1) were imaged at days 1, 4, 7, 11, 14, 18, and 21 during aggregate culture via light microscopy (Olympus CKX41 with Nikon DS-Fi2 camera and Nikon DS-L3 attachment).

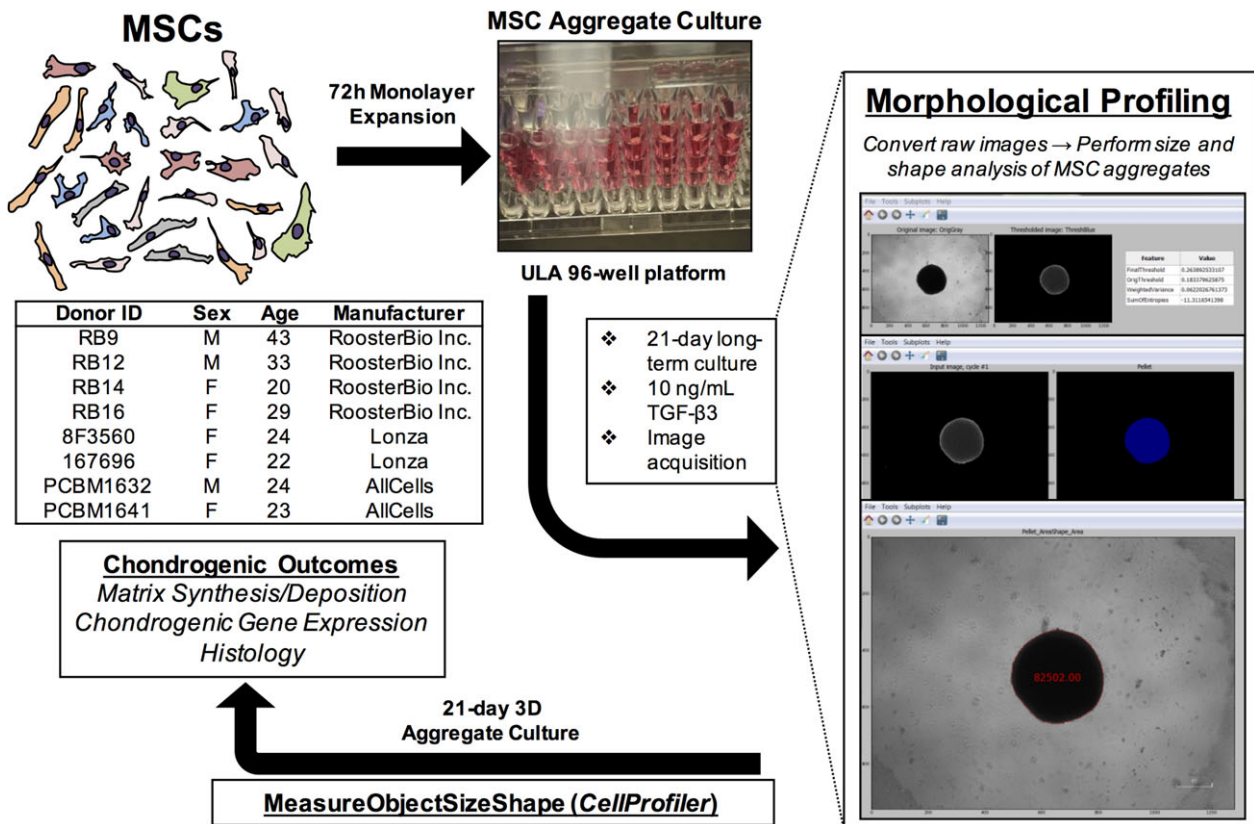


**Figure 1.** A schematic of the experimental workflow for the analysis of MSC chondrogenic capacity is shown. Using MSC lines derived from eight different donors at two passages each ( $n = 10\text{--}15$ ), we aim to primarily investigate the effects of cell passage on the morphological dynamics of formed MSC aggregates, how these morphological characteristics correlate with MSC chondrogenic capacity, and whether these effects are conserved across MSCs derived from multiple donors. MSCs at P2 or P3 and P5, respectively designated as early and late passage, are culture expanded for 72 hours and then formed into aggregates of defined size for 3D culture over 21 days. Images of aggregates are acquired and tracked during the culture period at various time points for morphological analysis using quantitative computational methods (CellProfiler). MSC aggregate morphological features (14 total) are then correlated with their respective chondrogenic outcomes, which are measured at day 21. Abbreviation: MSCs, multipotent stromal cells.

Automated analysis and quantification of morphological features were performed using the open-source image analysis software CellProfiler 2.2.0 to provide high-dimensional morphological characterization of MSC aggregates comprising 14 shape and size features (Supporting Information Table S1). The CellProfiler algorithm (pipeline) used to perform the morphological characterization can be viewed in Supporting Information Table S2. Principal component analysis (PCA) was performed to reduce these large multivariate morphological datasets into a smaller number of artificial (dimensionless) principal components (PC), which represent an uncorrelated linear combination of optimally weighted observed variables that capture maximal variance in the original dataset. From this PCA, only the first two PC were selected as they accounted for at least 70% of the cumulative explained variance of the original data.

### Quantitative Evaluation of Chondrogenic Capacity

At day 21, MSC aggregates were collected from spheroid culture and frozen at  $-20^{\circ}\text{C}$  until use for biochemical analysis. More detailed descriptions of this protocol are found in the Supporting Information.

DNA content, used as an indirect indicator of aggregate cellularity, was quantified using the Quant-iT PicoGreen dsDNA Assay Kit (Molecular Probes, Eugene, OR) according to the

manufacturer's protocols. Sulfated glycosaminoglycan (GAG) content, used as a direct indicator of extracellular matrix deposition and synthetic activity, was measured using the established 1,9-dimethylmethylene blue dye calorimetric assay as previously described [24]. To measure the synthetic activity of MSC aggregates, the resulting total GAG amounts from each sample were normalized to the total DNA amount from that same sample.

MSC aggregates were processed for real-time reverse transcriptase polymerase chain reaction (RT-PCR) to quantify the expression of selected genes as gauges for chondrogenic differentiation. Total RNA were isolated from samples using the RNeasy Mini Kit (Qiagen, Valencia, CA) following the manufacturer's protocols. The isolated RNA samples were reverse-transcribed into cDNA using the Verso cDNA Synthesis Kit (ThermoFisher Scientific, Waltham, MA), where the final cDNA transcripts were used for the quantification of selected genes listed in Supporting Information Table S3 [25, 26] by RT-PCR using established primers and Power SYBR Green Master Mix (Applied Biosystems, Foster City, CA).

PCA was performed on supervised datasets measuring chondrogenic outcomes to generate composite scores principle component 1 (PC1) that captures maximal variance in the data representing matrix synthetic activity (SynthAct; DNA, GAG, GAG/DNA) and chondrogenic gene expression (ChondroGene; type

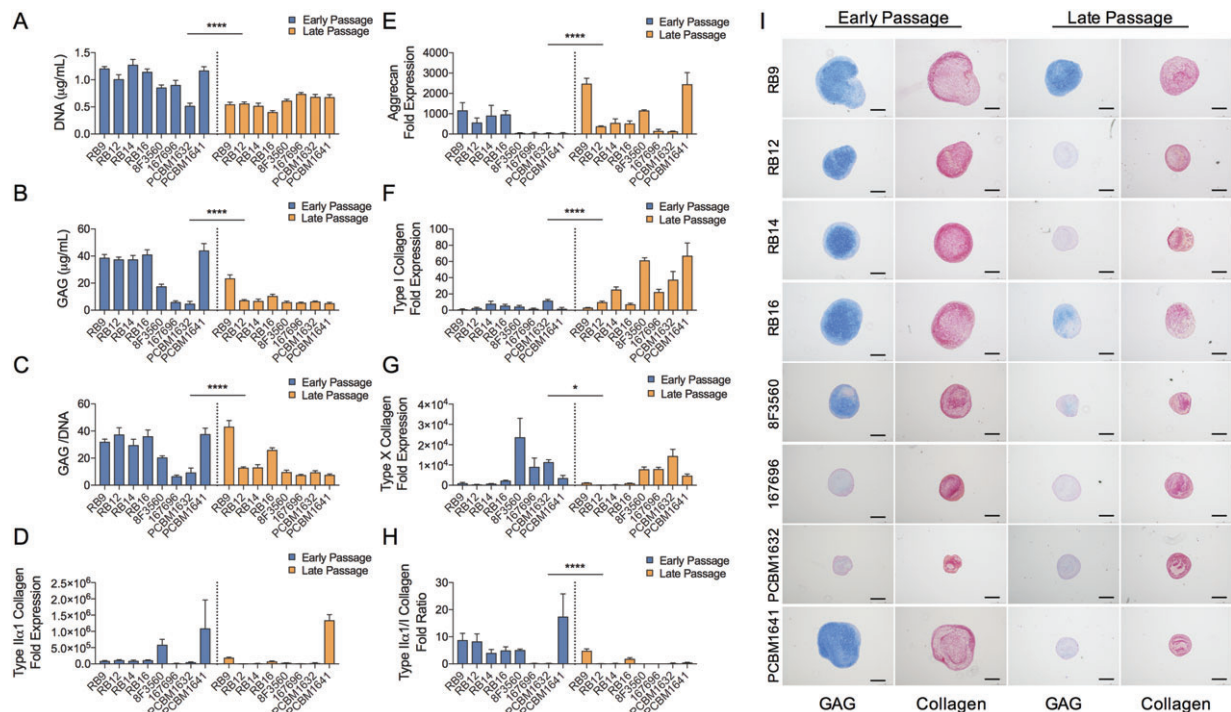


**Figure 2.** Following 21 days of 3D culture, the (A) DNA, (B) GAG, and (C) GAG/DNA were quantified using biochemical assays to provide an indirect measure of cellularity, matrix deposition, and matrix synthetic activity, respectively. Additionally, the expression levels of canonical chondrogenic genes, which include (D) type II $\alpha$ 1 collagen, (E) aggrecan, (F) type I collagen, (G) type X collagen, and the (H) type II $\alpha$ 1/I collagen fold ratio were also quantified. \* Indicates a statistically significant difference between early passage and late passage samples ( $p < .05$ , and  $****p < .0001$ , two-way ANOVA). Data are presented as the mean  $\pm$  SD values of the biological replicates included per group ( $n = 4$ ) for these analyses. (I): Histological sections of multipotent stromal cells aggregates illustrate GAG (blue) and collagen (red) distribution after 21 days in 3D culture. Scale bar = 500  $\mu$ m.

II $\alpha$ 1 collagen, aggrecan, and type II $\alpha$ 1/type I collagen fold ratio) of the MSCs. Unsupervised PCA was also performed on all available chondrogenic outcome measures to generate a composite metric that can be used as an overall chondrogenic index (Chondrolnd).

### Histology

More details regarding the processing of samples for histology are found in the Supporting Information. Raw histology images were then quantified using the CellProfiler algorithm shown in Supporting Information Table S4. Briefly, the total intensity quantified from the histological stains were normalized to the corresponding MSC spheroid area to account for differences in aggregate size.

### Gene Expression Microarray Hybridization, Data Acquisition, and Statistical Analysis

All gene expression microarray data files have been uploaded into the public repository, Gene Expression Omnibus (GSE110755). A more detailed description of the experimental and analytical methods used in this study are found in the Supporting Information.

## RESULTS

### Chondrogenic Synthetic Activity and Gene Expression Exhibit Cell Line- and Passage-Dependence

To assess the chondrogenic differentiation potential of each MSC line, we quantified cellularity (DNA content), matrix

production, and chondrogenic gene expression after 21 days of chondrogenic stimulation. Regarding the DNA content, EP MSC aggregates generally maintained higher cellularity when compared to LP MSC aggregates (Fig. 2A). Differences between MSC cell lines were more evident in terms of extracellular matrix production (as measured by GAG content). Despite exhibiting greater matrix production overall versus LP aggregates, not all EP MSC aggregates (8F3560, 167696, and PCBM1632) displayed high amounts of GAG deposition by D21 (Fig. 2B). Among LP aggregates, only RB9 and RB16 showed moderate amounts of GAG deposition. This pattern in GAG deposition became much more apparent when normalized to DNA. Of note, the normalized matrix production (GAG/DNA) of LP RB9 aggregates reached levels comparable to EP groups with high GAG production (Fig. 2C).

Gene expression profiling of well-known chondrogenic marker genes revealed trends between cell-lines and passages that deviated from the DNA and GAG content (Fig. 2D–2G). For instance, at EP, both 8F3560 and PCBM1641 aggregates showed the highest levels of type II $\alpha$ 1 collagen expression despite the former having produced the least amount of GAG (Fig. 2D). Other such discrepancies between synthetic activity and gene expression also appeared for the expression of aggrecan (Fig. 2E). For type I collagen expression, a cartilage dedifferentiation marker, LP aggregates generally maintained greater levels of expression compared to EP aggregates (Fig. 2F). MSC aggregates with low matrix production from both EP and LP groups displayed significantly increased type X collagen gene expression, a hypertrophic marker, when

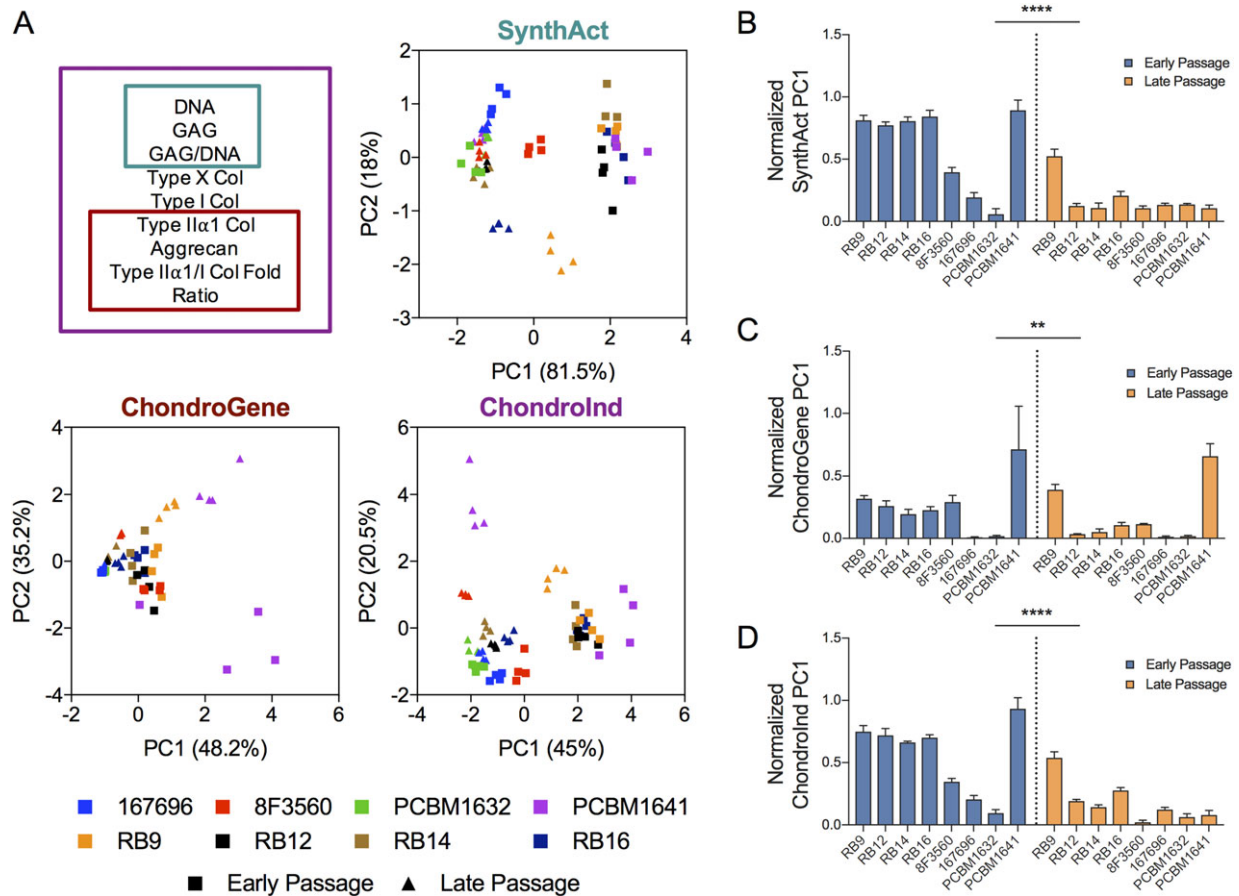


**Figure 3.** (A): PCA was performed using supervised datasets comprising metrics that include the greatest variability in synthetic activity (DNA, GAG, and GAG/DNA) and chondrogenic gene expression (type II $\alpha$ 1 collagen, aggrecan, and type II $\alpha$ 1/type I collagen fold ratio) as illustrated by the colored boxes. Unsupervised PCA was also performed on all outcome measurements to derive an overall quantitative composite score (ChondroInd) that captures aspects of both the actual synthetic activity as well as chondrogenic gene expression of multipotent stromal cell lines. Normalized PC1 scores from each PCA performed (supervised and unsupervised), which account for the greatest variance in SynthAct (81.5%), ChondroGene (48.2%), and ChondroInd (45%) datasets, are shown in (B), (C), and (D), respectively. \* Indicates a statistically significant difference between early passage and late passage samples (\*\* $p < .005$  and \*\*\*\* $p < .0001$ , two-way ANOVA). Data are presented as the mean  $\pm$  SD values of the biological replicates included per group ( $n = 4$ ) for these analyses.

compared to MSC lines of higher matrix production (Fig. 2G). When the type II $\alpha$ 1/I collagen fold ratio (Fig. 2H) was measured to indicate the extent of hyaline (as opposed to fibrous) cartilage differentiation, we observed that the pattern of this metric between groups generally paralleled that of their matrix production (Fig. 2I).

To further characterize MSC chondrogenesis, extracellular matrix deposition, and distribution was quantified using image analysis of histological sections of aggregates (Fig. 2I). At EP, six out of the eight MSC lines (RB9, RB12, RB14, RB16, 8F3560, and PCBM1641) displayed moderate-to-significant GAG deposition throughout the entire spheroid as indicated by the intense Alcian blue staining. Only two of these MSC lines, namely RB9 and RB16, showed histologically detectable GAG deposition at LP. Overall, quantified GAGs from the histology correlated very strongly with biochemically detected GAGs (Supporting Information Fig. S1A). Most MSC lines display moderate-to-high amounts of collagen deposition at both EP and LP, especially at the periphery of the chondrogenically stimulated aggregates. Although EP aggregates produced more total collagen than LP aggregates, the quantified collagen from the histology yielded no apparent patterns between MSC lines

and did not correlate with biochemically measured GAG matrix production (Supporting Information Fig. S1B).

### Generation of a Composite Quantitative Metric for Overall Chondrogenic Capacity

As singular measures from individual assays may not fully elucidate the extent of MSC chondrogenic differentiation, we used PCA to integrate multiple assay outcomes into single quantitative values representing both overall and key aspects of chondrogenic potential. Supervised PCA was performed as outlined in Figure 3A, where the PC accounting for the maximum observed variance (PC1) from each respective PCA was used to construct quantitative composite measures of collective chondrogenic synthetic activity (DNA, GAG, and GAG/DNA) and chondrogenic gene expression (type II $\alpha$ 1 collagen, aggrecan, and type II $\alpha$ 1/I collagen fold ratio), referred to as the SynthAct and ChondroGene scores, respectively. Type I collagen and type X collagen were not included in the derivation of the ChondroGene scores as their inclusion resulted in decreased captured variance in the first two PC scores for the dataset (i.e., 83.4% vs. 62.9% of captured variance), making the use of a single composite score representative of

chondrogenic gene expression difficult (Fig. 3, Supporting Information Fig. S2A). Furthermore, increases in type I collagen and type X collagen expression, unlike the other chondrogenic gene expression metrics, do not reflect hyaline-like chondrogenic differentiation but rather dedifferentiation and hypertrophy, respectively. Overall MSC chondrogenic potential, referred to as the ChondroInd, is then measured by PC1 of the unsupervised PCA performed on all outcome measures (including type I collagen and type X collagen) and embodies the greatest amount of variance in the unsupervised dataset at 45%. When experimental results representing various aspects of MSC chondrogenic differentiation were plotted in PC space, we observed clear separations between experimental groups, indicating the use of raw PC scores as a viable method for assessing MSC chondrogenic potential.

For improved clarity, the derived chondrogenic composite scores were then rescaled via normalization to remove negative values (Fig. 3B–3D). By compartmentalizing MSC chondrogenic differentiation into individual metrics for chondrogenic synthetic activity and gene expression, we observed that while EP MSC aggregates maintained much higher SynthAct scores over LP aggregates (Fig. 3B), the same pattern was not observed for ChondroGene scores (Fig. 3C). For SynthAct, MSC groups exhibited scores that matched the observed matrix deposition from the histological analysis. However, there were notable inconsistencies in the ChondroGene scores as some LP groups (PCBM1641 and 8F3560) displayed increased ChondroGene scores despite possessing correspondingly low SynthAct scores. Indeed, the SynthAct scores were only weakly correlated with the ChondroGene scores (Supporting Information Fig. S2B). Additionally, both histomorphometrically derived metrics for GAGs and collagen either weakly correlated or failed to correlate with chondrogenic gene expression, respectively (Supporting Information Fig. S2C). Despite this mismatch, the overall ChondroInd, which incorporates both SynthAct and ChondroGene, provided differences between MSC groups that were more congruent with their expressed phenotype (Fig. 3D), highlighting the utility of such a composite score for quantifying the degree of overall MSC chondrogenic differentiation.

### Morphological Profiling of MSC Aggregates Reveal Cell Line- and Passage-Dependent Differences in Aggregate Size and Shape Change

In our study, culture-expanded MSCs (from eight different donors at EP and LP) were formed into aggregates and stimulated with standard chondrogenic induction medium to assess MSC chondrogenic capacity in tandem with morphological profiling, where high-dimensional morphological features were quantified at various time points. Unsupervised PCA was performed (using all 14 morphological features) to reduce the multivariate dataset into two PC scores, with PC1 and PC2 capturing 61.2% and 23.2% of the morphological data variance, respectively. From the factor loading plot, size-based parameters were more highly correlated with PC1 while shape-based parameters were more highly correlated with PC2 (Supporting Information Fig. S3). As a result, PC1 (Size) and PC2 (Shape) represent overall morphological scores that relate to MSC aggregate size and shape, respectively. Therefore, we assessed whether these scores could be used to determine 3D morphological dynamics of different cell-lines and passages following chondrogenic stimulation (Fig. 4A).

Several MSC lines at LP demonstrated incomplete aggregation into spheroids as indicated by high Day 1 PC1 (Size) scores (Fig. 4A). While most MSC aggregates decreased in size by Day 4, several MSC aggregates exhibited size increases after this time point where EP aggregates continuously maintained larger sizes when compared to LP aggregates. Comparing PC1 (Size) scores beginning at Day 1, differences in aggregate size due to donor variations became readily apparent, where different morphological trends also emerged depending on passage. By Day 21, the same five larger EP groups (RB9, RB12, RB14, RB16, and PCBM1641) had exhibited continued increases in size over time whereas the initially smaller EP groups (167696 and PCBM1632) had further compacted during culture. Although most LP MSC lines continued to decrease in size until Day 21, one LP group (RB9) grew significantly larger and was comparable in size to aggregates from other EP MSC lines. There were no discernible trends in PC2 (Shape) dynamics with respect to cell line or passage except for RB12 (Supporting Information Fig. S4). Indeed, shape differences between MSC lines were not apparent until Day 14. Representative aggregates from all MSC lines at Days 7 and 21 are shown in Figure 4B.

We next investigated cell line variations in the morphological dynamics of MSC aggregates by mapping the raw PC1 (Size) and PC2 (Shape) scores over the entire culture duration for each MSC line (Fig. 5A). We immediately observed from their morphological trajectories (Fig. 5B) that RB14, PCBM1641, and to an extent 8F3560 MSCs shared very similar changes in aggregate morphologies over time. EP and LP aggregates from these cell lines were all similarly sized at the beginning of culture but then significantly diverged in size after Day 4. Unlike RB14 and PCBM1641, however, EP 8F3560 aggregates did not surpass their original size at D1 over time. RB16 and RB12 shared similar morphological dynamics in that both their LP aggregates were initially larger and differently shaped (due to incomplete aggregation) compared to EP aggregates. Over time, LP RB16 and RB12 aggregates became more spherical but decreased significantly in size when compared to EP aggregates, which grew larger than their Day 1 counterparts. 167696 and PCBM1632 aggregates showed very comparable morphological profiles, where both EP and LP aggregates diminished significantly in size after Day 7. The RB9 cell line was unique in that both EP and LP aggregates regained size over time after an initial decrease.

### Morphological Phenotypes Emerge upon Chondrogenic Stimulation That Predict Overall Chondrogenic Capacity

To identify emergent MSC aggregate morphological phenotypes predictive of chondrogenic capacity, correlations were made between MSC morphological scores at each time point and their measures of chondrogenic differentiation (Fig. 6). Raw scores were rescaled via normalization prior to plotting to remove negative values for improved clarity. We observed that PC1 (Size) scores became strongly correlated with the SynthAct and ChondroInd scores as early as Day 7 (Fig. 6A), where  $R$  values exceeded 0.8 after 1 week of culture for both SynthAct and ChondroInd measures. However, variability in MSC aggregate size-based morphological features did not correlate with ChondroGene scores at any time point. In contrast to PC1 (Size) scores, the PC2 (Shape) scores achieved statistically significant correlations with SynthAct and ChondroInd scores much later at Day 14 and beyond (Fig. 6B). Furthermore, correlations between PC2 (Shape) scores and the chondrogenic outcomes were not as

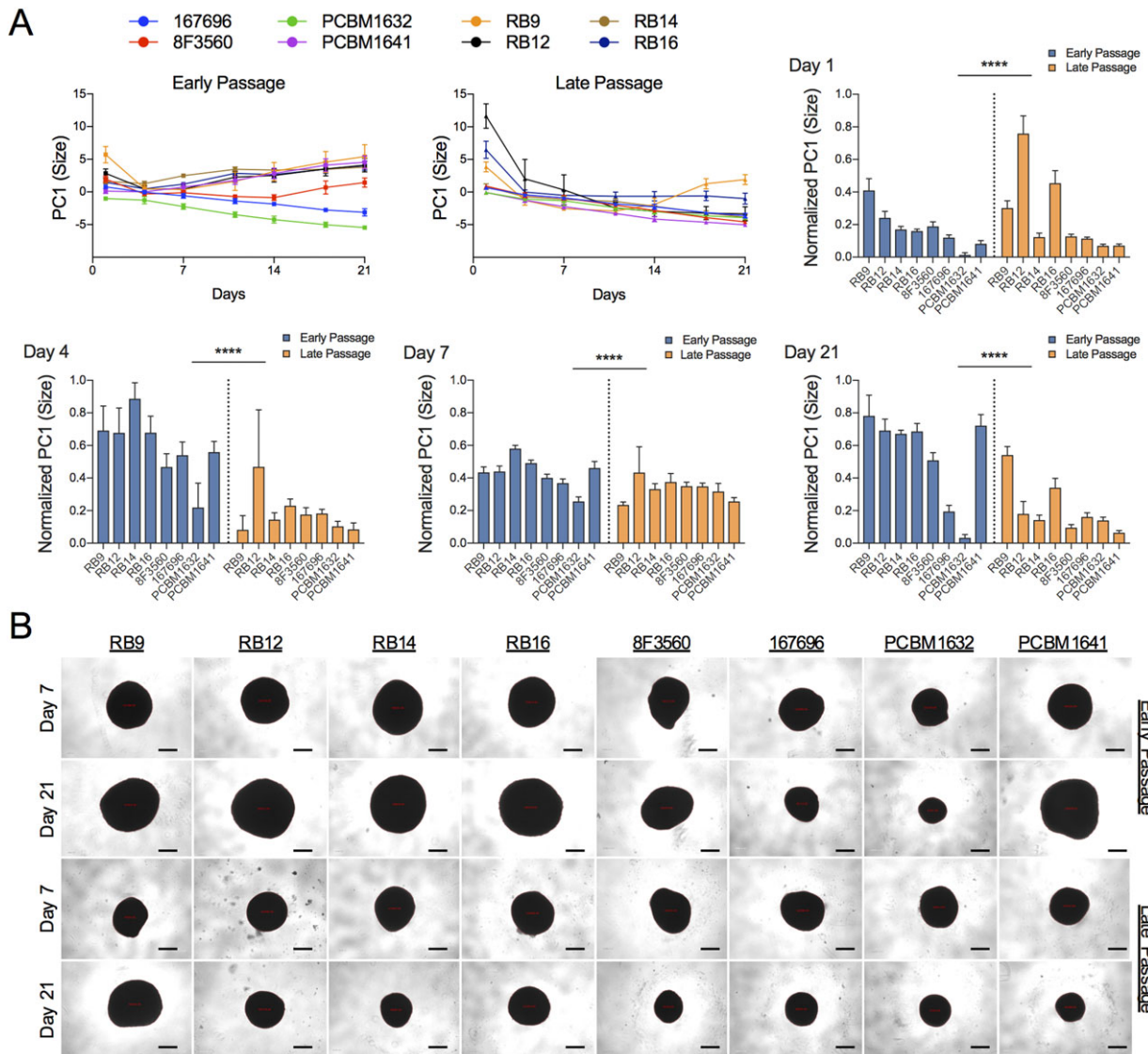


**Figure 4.** (A): Multipotent stromal cell (MSC) aggregates exhibit different patterns in aggregate size changes, as represented by the PC1 score derived from the PCA performed on the entire morphological dataset, during the culture period depending on both the cell line and passage. The PC1 (Size) scores of the aggregates were compared between early and late passage groups and shown at Day 1, Day 4, Day 7, and Day 21. \* Indicates a statistically significant difference between early passage and late passage samples (\*\*\*\* $p < .0001$ , two-way ANOVA). Data are presented as the mean  $\pm$  SD values of the biological replicates included per group ( $n = 10\text{--}15$ ) for the experiments. Bright-field images depicting the MSC aggregates from each group at Day 7 and Day 21 and at both passages for each time point are shown in (B). Scale bar = 500  $\mu\text{m}$ .

strong as those for PC1 (Size) scores (lower  $R$  values). As was the case for PC1 (Size) scores, PC2 (Shape) scores did not correlate with ChondroGene scores at any time point.

Individual morphological features measuring both MSC aggregate size and shape were also independently correlated with the multiple chondrogenic metrics to elucidate which morphological feature may be most indicative of MSC chondrogenic potential. While most of the size-based morphological features became significantly correlated with SynthAct and the ChondroInd by Day 7, the three measures of aggregate radii (MaxRadius, MeanRadius, and MedianRadius) were already strongly correlated by Day 4 (Supporting Information Table S5). Correlations between some shape-based features and the chondrogenic metrics including the ChondroGene scores were also observed, namely at Day 11. Of the multiple

shape-based morphological features measured, only the form factor (i.e., circularity) maintained significant correlations with the SynthAct, ChondroGene, and ChondroInd scores at Day 11, where less circular spheroids tended to have higher chondrogenic potential (Supporting Information Table S6).

#### Gene Expression of Undifferentiated MSCs Correlate with Measures of Chondrogenic Differentiation

Global gene microarray analysis (62,976 probes) was performed on the MSC lines without chondrogenic stimulation to identify inherent differences in gene expression that may correlate with their chondrogenic capacity. 750 probes were found to be significantly different when comparing EP versus LP MSCs (Supporting Information Table S7), where only 32 genes exhibited absolute

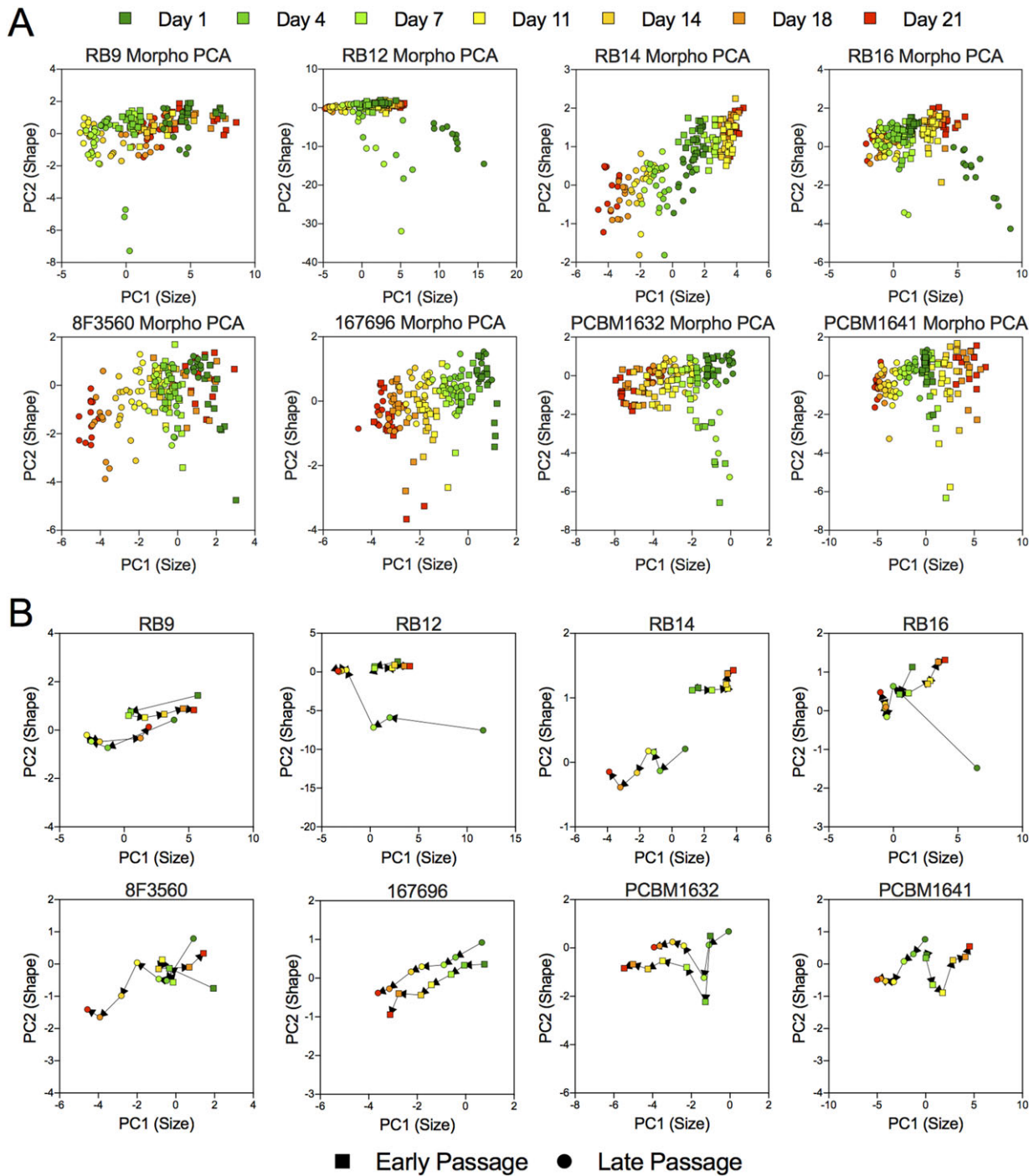


**Figure 5.** (A): The dynamics of the multipotent stromal cell aggregate size and shape over the culture period are shown for each cell line, where (B) the mean trajectory in morphology PC scores for each cell line are also tracked over time for both early and late passage groups.

fold changes greater than 1.5 (Supporting Information Fig. S5A). When MSC lines were grouped and compared according to higher (RB9EP/LP, RB12EP, RB14EP, RB16EP/LP, PCBM1641EP, 8F3560EP) or lower (RB12LP, RB14LP, PCBM1641LP, 8F3560LP, PCBM1632EP/LP, 167696EP/LP) chondrogenic potential (based on ChondroInd; cutoff value set by RB16LP), 66 probes were identified (Supporting Information Table S8) to be either significantly upregulated or downregulated (Supporting Information Fig. S5B). When correlating the microarray data of the undifferentiated MSC

lines with the corresponding ChondroInd scores following chondrogenic stimulation, a total of 107 probes were observed to be statistically significant (Supporting Information Fig. S5C; Supporting Information Table S9). A preliminary pathway analysis was also performed to identify associated biofunctions (Supporting Information Table S10). A hierarchical clustering heat map was generated to illustrate differences in gene expression, where MSC lines are ordered from high to low chondrogenic potential based on ChondroInd scores (Fig. 7).



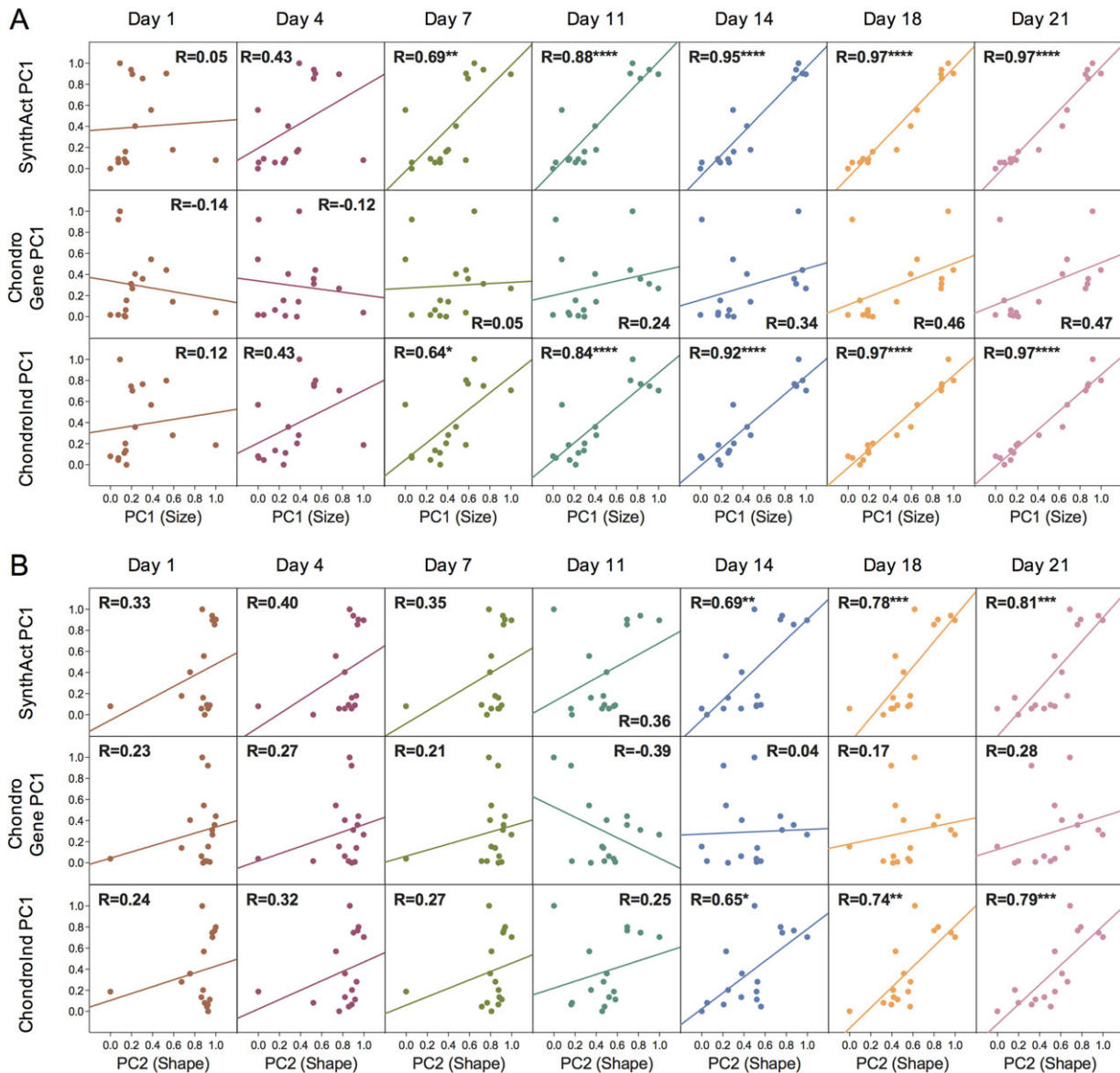


**Figure 6.** Normalized PC1 scores representing MSC synthetic activity, chondrogenic gene expression, and overall chondrogenic index were correlated with **(A)** PC1 (Size) and **(B)** PC2 (Shape) morphology scores at various time points measured during the 21-day aggregate culture. The correlation coefficient  $R$  measures the strength of the linear relationship between correlated variables, where \* indicates a statistically significant correlation ( $*p < .05$ ,  $**p < .005$ ,  $***p < .0005$ , and  $****p < .0001$ , Pearson product-moment correlation).

## DISCUSSION

MSC heterogeneity represents a major obstacle to establishing critical quality attributes that can effectively predict the functional capacity of MSCs relevant to therapeutic applications such as chondrogenesis. MSC functional heterogeneity (differences in therapeutic function [17]) across donors and even within a single population can derive from both intrinsic and extrinsic factors [19], the latter of which also include various manufacturing parameters (i.e., different cell isolation/expansion protocols, general media composition, and other operator effects). New innovative approaches have begun to correlate the morphology of MSC subpopulations within larger populations to their differentiation (adipogenic and osteogenic) [20, 21] and immunosuppressive [23] potential. While several culture methods and assays for characterizing MSC

chondrogenic differentiation do exist [27, 28], there still lacks well-defined approaches that seek to identify cell critical quality attributes predictive of MSC chondrogenic potential. Toward this goal, we characterized the morphology of MSC aggregates under chondrogenic stimulation from multiple donors and demonstrated that MSC aggregates in 3D culture exhibited unique morphological dynamics that were both passage and cell line dependent. We showed that MSC chondrogenic differentiation becomes highly correlated with size-based features of formed aggregates much earlier during 3D culture versus shape-based features, suggesting the ability to use quantitative aggregate morphology as a simple tool to estimate the chondrogenic capacity of an MSC line.

MSC heterogeneity is still often overlooked as many research groups continue to generalize the regenerative potential of selected cell lines to all MSCs [18]. However,

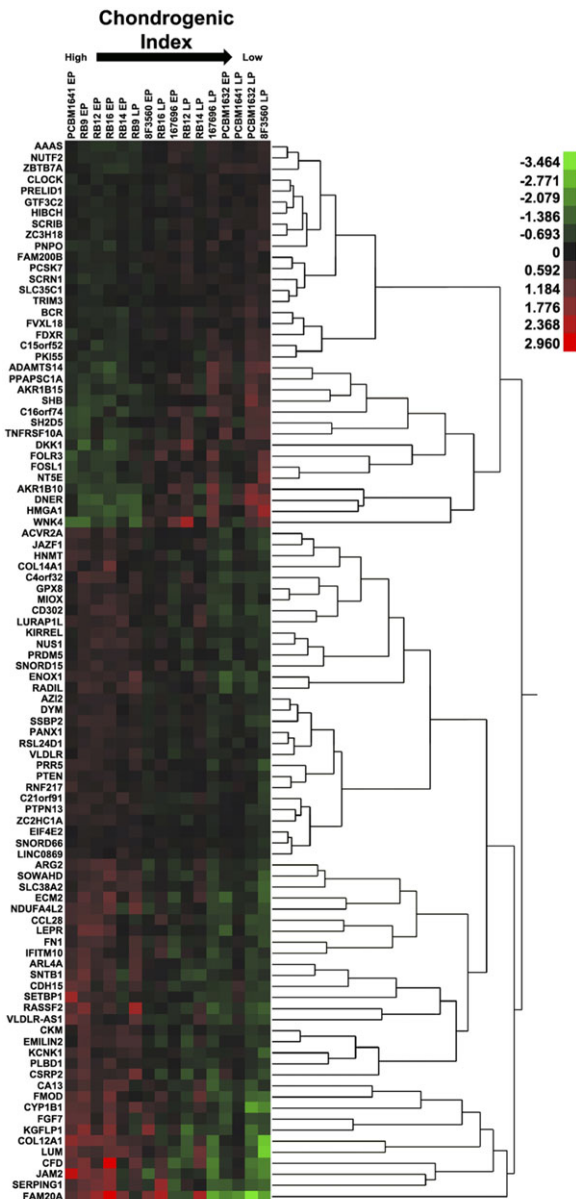


**Figure 7.** Hierarchical clustering heat map illustrates gradual increases and decreases in the expression of genes in undifferentiated multipotent stromal cells (MSCs) found to be significantly correlated with their ChondroInd scores at Day 21. MSC lines are ordered from highest to lowest chondrogenic potential based on ChondroInd scores.

research efforts have been more recently focused on the characterization of MSC heterogeneity with the hope of developing adaptable tools using certain quality attributes for predicting cell behavior. Comparing eight different MSC lines, it was shown that undifferentiated MSCs isolated from different donors exhibited varying colony-forming unit (CFU) capacities [29], indicating varying degrees of stemness. Yet, stemness levels as measured by both %CFU and flow cytometry (for MSC surface markers) did not reflect their ability to undergo adipogenic differentiation, highlighting inadequacies in the use of cell surface markers alone as a biomarker for MSCs (a common practice). Recent efforts characterizing the gene

expression profile of proliferating MSCs via microarray analysis also showed that gene expression changes associated with MSC aging during passage failed to correspond with any of the markers established by the International Society for Cellular Therapy [30, 31]. However, the identification of new epigenetic [32] and genetic markers [33] correlated with cell function could provide quality tools for assaying MSC potency.

One significant advantage of our investigation involves the use of multiple MSC lines that were also previously evaluated for differences in their adipogenic [29], osteogenic [20], proliferative [30], and immunosuppressive [23] capacities. It was noted previously that while the proliferative patterns (time to confluency, cell size, and morphology) of MSCs were similar at earlier passages [29, 33, 34], they began to diverge at later passages as the MSCs derived from various donor source exhibited differential gene expression of markers indicative of senescence [30]. However, MSCs manufactured from different donor sources exhibited differences in genetic stability and varied in adipogenic, osteogenic, and immunosuppressive potential regardless of passage. Unlike the referred studies, we evaluated MSCs in 3D culture where variations in the observed readouts may potentially reflect dissimilarities in cellular processes originating from mesenchymal condensation. Previous studies have shown that MSCs cultured as 3D spheroids versus 2D monolayers improved overall survival [35] and increased their functional tropism [36]. Although not directly tested in our case, it is a possibility that the transition from 2D monolayers to 3D spheroids did not elicit the same universal response in all MSCs. We noted that under similar chondrogenic conditions, six out of eight MSC lines produced significant amounts of GAG at EP whereas only two out of eight MSC lines displayed any GAG production at LP. Interestingly, histological analysis performed on MSC groups with high GAG production (at both passages) revealed not only larger aggregates overall but also extracellular matrix distributions similar to native articular cartilage; GAGs were deposited more densely at the aggregate core while collagens were more heavily aligned along the spheroid periphery. Such was not the case for MSC groups presenting minimal extracellular matrix production where the GAG deposition overlapped with that of collagen. This perhaps indicates an impaired ability of these MSCs to rearrange their aggregate packing density for metabolic adaptation [35], which merits further investigation.

As it was previously shown that the mRNA expression of the canonical gene aggrecan failed to correlate with MSC matrix production at the single-cell level [37], we developed an approach using PCA to segregate metrics of chondrogenic differentiation into individual composite scores representative of chondrogenic synthetic activity (SynthAct) and gene expression (ChondroGene). We evaluated the correlation between functional chondrogenic differentiation and MSC aggregate morphology, a phenotypic readout that can be readily measured over time using nondestructive imaging techniques. Although some studies have peripherally explored the association between MSC spheroid morphology and differentiation states [9, 38], few attempts have since been made at establishing quantitative relationships. While our study used 2D projections of multicellular spheroids for high-dimensional morphological analysis, the evaluation of volumetric spheroid morphology [39] could potentially provide further biological insight. Compared to larger MSC aggregates, smaller MSC aggregates may consist of MSC populations containing more

subpopulations of highly contractile cells that led to overall greater aggregate compaction, which requires further study. Indeed, histological examination of smaller aggregates generally revealed more collagen deposition at the aggregate cores, indicating perhaps the increased cortical tension and cell-matrix interactions characteristic of more contractile cells [40]. These results suggest the strong possibility of adapting this phenotypic readout for quickly estimating functional chondrogenic matrix accumulation in lieu of other more costly and arduous processes. Delay in the time to correlation, as well as lower correlation strengths, between aggregate shape and measures of chondrogenic functional capacity point to a disconnect between cell spheroid size and spheroid shape that may be of biological interest. Additionally, the lack of any correlation between ChondroGene and aggregate morphology at any time point further highlights the need to establish a phenotypic basis in chondrogenic gene expression.

Despite significant discrepancies between the chondrogenic gene expression data and phenotypic outcomes (i.e., synthetic activity and histology), we further explored potential genetic signatures of MSC lines prechondrogenic induction that may be indicative of chondrogenic potential. Of the 107 probes (out of 62,976) found to be significantly correlated with the ChondroInd of the MSC cohort, a number of prominent genes were identified in the literature to be implicated in several biological functions related to cell–cell signaling, tissue and organ morphology, and musculoskeletal development. Given the varying dynamics observed in MSC aggregate morphology, which embodies a form of organoid culture, it is expected that such biological functions were found to be associated with chondrogenic potential. Genes found to be positively (JAM2, COL12A1, LUM, and FGF7) and negatively (DNER, DKK1, ADAMTS14, and SHB) correlated with ChondroInd suggest that MSCs of higher chondrogenic capacity may be inherently more migratory, more efficient at matrix reorganization, and more metabolically adaptable [41–46], which prompted further investigation. Comparing EP and LP MSCs, genes revealed to be differentially expressed largely corroborated previous data comparing the effects of passage in other MSC lines [30, 33]. While we provide an exploratory analysis of the relationship between MSC chondrogenic phenotype and their source gene expression, a more comprehensive genomic analysis could reveal gene signatures predictive of MSC chondrogenic potential, which is the topic of our ongoing work.

## CONCLUSION

In summary, we demonstrated that multiple MSC lines exhibited both cell line- and passage-dependent aggregate morphologies during spheroid culture that correlated strongly with chondrogenic capacity. Using temporal high-dimensional morphological analysis of MSC aggregates, we created composite

scores for morphological data based on size and shape morphological features, which were used to show that aggregates formed by MSCs from different donors diverged more in size than shape between cell lines following chondrogenic stimulation. Applying similar methodology for the analysis of chondrogenic outcomes, we further derived quantitative scores to represent the individual as well as combined matrix accumulation and gene expression aspects of chondrogenic differentiation. We showed via correlation analysis that functional matrix accumulation (SynthAct) but not chondrogenic gene expression (ChondroGene) correlated strongly with aggregate morphology as early as Day 7, highlighting a discrepancy between chondrogenic phenotype and gene expression. Furthermore, MSC aggregate size correlated with chondrogenic synthetic activity much earlier than MSC aggregate shape, which became significantly correlated by Day 14. Correlation of these phenotypic data with base gene expression of unstimulated MSCs featured several biological pathways and markers that provide key starting points for future research endeavors toward assaying MSCs. Finally, by developing a simple nondestructive approach demonstrating a strong correlation between early MSC aggregate morphology and chondrogenic potential, we provide a well-defined tool for the early estimation of MSC chondrogenic differentiation capacity. Indeed, the simple measurement of MSC aggregate morphology represents a useful resource for the improvement of quality for manufactured cell products.

## ACKNOWLEDGMENTS

This work was supported in part by Dr. Johnny Lam's appointment to the Research Participation Program at CBER administered by the Oak Ridge Institute for Science and Education through the US Department of Education and US Food and Drug Administration. This work was also partially supported by the Food and Drug Administration Modernizing Science grant program and research funds from the Division of Cellular and Gene Therapies.

## AUTHOR CONTRIBUTIONS

J.L. and K.E.S.: conceived and designed the research; J.L., I.H.B., and R.A.M.: performed the experiments and data analysis; J.L., I.H.B., R.A.M., S.R.B., R.K.P., and K.E.S.: contributed intellectual input and critically reviewed and wrote the manuscript.

## DISCLOSURE OF POTENTIAL CONFLICTS OF INTEREST

The authors indicated no potential conflicts of interest.

## REFERENCES

- 1 Armiento AR, Stoddart MJ, Alini M et al. Biomaterials for articular cartilage tissue engineering: Learning from biology. *Acta Biomater* 2018;65:1-20.
- 2 Lai WM, Hou JS, Mow VC. A triphasic theory for the swelling and deformation

behaviors of articular cartilage. *J Biomech Eng* 1991;113:245-258.

- 3 Sophia Fox AJ, Bedi A, Rodeo SA. The basic science of articular cartilage: structure, composition, and function. *Sports Health* 2009;1:461-468.

- 4 Cross M, Smith E, Hoy D et al. The global burden of hip and knee osteoarthritis:

estimates from the global burden of disease 2010 study. *Ann Rheum Dis* 2014;73:1323-1330.

- 5 Schnabel M, Marlovits S, Eckhoff G et al. Dedifferentiation-associated changes in morphology and gene expression in primary human articular chondrocytes in cell culture. *Osteoarthritis Cartilage* 2002;10:62-70.

- 6 Kolf CM, Cho E, Tuan RS. Mesenchymal stromal cells. *Biology of adult mesenchymal stem cells: regulation of niche, self-renewal and differentiation*. *Arthritis Res Ther* 2007; 9:204.
- 7 Pittenger MF, Mackay AM, Beck SC et al. Multilineage potential of adult human mesenchymal stem cells. *Science* 1999;284: 143-147.
- 8 Ichinose S, Tagami M, Muneta T et al. Morphological examination during in vitro cartilage formation by human mesenchymal stem cells. *Cell and Tissue Research* 2005; 322:217-226.
- 9 Arufe MC, De la Fuente A, Fuentes-Boquete I et al. Differentiation of synovial CD-105(+) human mesenchymal stem cells into chondrocyte-like cells through spheroid formation. *J Cell Biochem* 2009;108: 145-155.
- 10 Sekiya I, Vuorio JT, Larson BL et al. In vitro cartilage formation by human adult stem cells from bone marrow stroma defines the sequence of cellular and molecular events during chondrogenesis. *Proc Natl Acad Sci U S A* 2002;99:4397-4402.
- 11 Tuli R, Tuli S, Nandi S et al. Transforming growth factor-beta-mediated chondrogenesis of human mesenchymal progenitor cells involves N-cadherin and mitogen-activated protein kinase and Wnt signaling cross-talk. *J Biol Chem* 2003;278:41227-41236.
- 12 DeLise AM, Fischer L, Tuan RS. Cellular interactions and signaling in cartilage development. *Osteoarthritis Cartilage* 2000;8: 309-334.
- 13 Hall BK, Miyake T. All for one and one for all: condensations and the initiation of skeletal development. *Bioessays* 2000;22:138-147.
- 14 Lee JJ, Sato M, Kim HW et al. Transplantation of scaffold-free spheroids composed of synovium-derived cells and chondrocytes for the treatment of cartilage defects of the knee. *Eur Cell Mater* 2011;22:275-290.
- 15 Leijten J, Teixeira LS, Bolander J et al. Bioinspired seeding of biomaterials using three dimensional microtissues induces chondrogenic stem cell differentiation and cartilage formation under growth factor free conditions. *Sci Rep* 2016;6:36011.
- 16 Nakagawa Y, Muneta T, Otabe K et al. Cartilage Derived from Bone Marrow Mesenchymal Stem Cells Expresses Lubricin In Vitro and In Vivo. *PLoS ONE* 2016;11:e0148777.
- 17 Phinney DG. Functional heterogeneity of mesenchymal stem cells: implications for cell therapy. *J Cell Biochem* 2012;113: 2806-2812.
- 18 McLeod CM, Mauck RL. On the origin and impact of mesenchymal stem cell heterogeneity: new insights and emerging tools for single cell analysis. *European Cells and Materials* 2017;34:217-231.
- 19 Marklein RA, Lam J, Guvendiren M et al. Functionally-Relevant Morphological Profiling: A Tool to Assess Cellular Heterogeneity. *Trends Biotechnol* 2017;36:105-118.
- 20 Marklein RA, Lo Surdo JL, Bellayr IH et al. High Content Imaging of Early Morphological Signatures Predicts Long Term Mineralization Capacity of Human Mesenchymal Stem Cells upon Osteogenic Induction. *STEM CELLS* 2016;34:935-947.
- 21 Treiser MD, Yang EH, Gordonov S et al. Cytoskeleton-based forecasting of stem cell lineage fates. *Proceedings of the National Academy of Sciences of the United States of America* 2010;107:610-615.
- 22 Chen Y-Q, Liu Y-S, Liu Y-A et al. Biochemical and physical characterizations of mesenchymal stromal cells along the time course of directed differentiation. *Scientific Reports* 2016;6:31547.
- 23 Klinker MW, Marklein RA, Lo Surdo JL et al. Morphological features of IFN- $\gamma$ -stimulated mesenchymal stromal cells predict overall immunosuppressive capacity. *Proceedings of the National Academy of Sciences* 2017; 114:E2598-E2607.
- 24 Farndale RW, Buttle DJ, Barrett AJ. Improved quantitation and discrimination of sulphated glycosaminoglycans by use of dimethylmethylene blue. *Biochim Biophys Acta* 1986;883:173-177.
- 25 Koh RH, Jin Y, Kang BJ et al. Chondrogenically primed tonsil-derived mesenchymal stem cells encapsulated in riboflavin-induced photocrosslinking collagen-hyaluronic acid hydrogel for meniscus tissue repairs. *Acta Biomater* 2017;53:318-328.
- 26 Rothrauff BB, Shimomura K, Gottardi R et al. Anatomical region-dependent enhancement of 3-dimensional chondrogenic differentiation of human mesenchymal stem cells by soluble meniscus extracellular matrix. *Acta Biomater* 2017;49:140-151.
- 27 Farrell MJ, Shin JJ, Smith LJ et al. Functional consequences of glucose and oxygen deprivation on engineered mesenchymal stem cell-based cartilage constructs. *Osteoarthritis Cartilage* 2015;23:134-142.
- 28 Penick KJ, Solchaga LA, Welter JF. High-throughput aggregate culture system to assess the chondrogenic potential of mesenchymal stem cells. *Biotechniques* 2005;39: 687-691.
- 29 Lo Surdo JL, Millis BA, Bauer SR. Automated microscopy as a quantitative method to measure differences in adipogenic differentiation in preparations of human mesenchymal stromal cells. *Cytotherapy* 2013;15: 1527-1540.
- 30 Bellayr IH, Catalano JG, Lababidi S et al. Gene markers of cellular aging in human multipotent stromal cells in culture. *Stem Cell Research & Therapy* 2014;5:59.
- 31 Krampera M, Galipeau J, Shi Y et al. Immunological characterization of multipotent mesenchymal stromal cells--The International Society for Cellular Therapy (ISCT) working proposal. *Cytotherapy* 2013;15:1054-1061.
- 32 Lynch PJ, Thompson EE, McGinnis K et al. Chromatin Changes at the PPAR- $\gamma$ 2 Promoter During Bone Marrow-Derived Multipotent Stromal Cell Culture Correlate With Loss of Gene Activation Potential. *STEM CELLS* 2015;33:2169-2181.
- 33 Bellayr IH, Marklein RA, Lo Surdo JL et al. Identification of Predictive Gene Markers for Multipotent Stromal Cell Proliferation. *STEM CELLS DEV* 2016;25:861-873.
- 34 Lo Surdo J, Bauer SR. Quantitative approaches to detect donor and passage differences in adipogenic potential and clonogenicity in human bone marrow-derived mesenchymal stem cells. *Tissue Engineering Part C: Methods* 2012;18:877-889.
- 35 Murphy KC, Hung BP, Browne-Bourne S et al. Measurement of oxygen tension within mesenchymal stem cell spheroids. *Journal of The Royal Society Interface* 2017; 14:20160851-20160810.
- 36 Bartosh TJ, Ylostalo JH, Mohammadipoor A et al. Aggregation of human mesenchymal stromal cells (MSCs) into 3D spheroids enhances their antiinflammatory properties. *Proc Natl Acad Sci U S A* 2010;107:13724-13729.
- 37 Cote AJ, McLeod CM, Farrell MJ et al. Single-cell differences in matrix gene expression do not predict matrix deposition. *Nat Commun* 2016;7:10865.
- 38 Baraniak PR, McDevitt TC. Scaffold-free culture of mesenchymal stem cell spheroids in suspension preserves multilineage potential. *Cell Tissue Res* 2012;347:701-711.
- 39 Piccinini F, Tesei A, Arienti C et al. Cancer multicellular spheroids: volume assessment from a single 2D projection. *Comput Methods Programs Biomed* 2015;118:95-106.
- 40 Sart S, Tsai A-C, Li Y et al. Three-dimensional aggregates of mesenchymal stem cells: cellular mechanisms, biological properties, and applications. *Tissue Engineering Part B: Reviews* 2014;20:365-380.
- 41 Arcangeli ML, Frontera V, Aurand-Lions M. Function of junctional adhesion molecules (JAMs) in leukocyte migration and homeostasis. *Arch Immunol Ther Exp (Warsz)* 2013;61:15-23.
- 42 Huang T, Wang L, Liu D et al. FGF7/FGFR2 signal promotes invasion and migration in human gastric cancer through upregulation of thrombospondin-1. *Int J Oncol* 2017;50:1501-1512.
- 43 Leijten J, Georgi N, Moreira Teixeira L et al. Metabolic programming of mesenchymal stromal cells by oxygen tension directs chondrogenic cell fate. *Proc Natl Acad Sci U S A* 2014;111:13954-13959.
- 44 Ling L, Nurcombe V, Cool SM. Wnt signaling controls the fate of mesenchymal stem cells. *Gene* 2009;433:1-7.
- 45 Park JR, Jung JW, Seo MS et al. DNER modulates adipogenesis of human adipose tissue-derived mesenchymal stem cells via regulation of cell proliferation. *Cell Prolif* 2010;43:19-28.
- 46 Shaw LM, Olsen BR. FACIT collagens: diverse molecular bridges in extracellular matrices. *Trends Biochem Sci* 1991;16: 191-194.



See [www.StemCellsTM.com](http://www.StemCellsTM.com) for supporting information available online.